Synthesis of Porous and Graphitic Carbon for Electrochemical Detection

4 AUTHORS, INCLUDING:

Wei Li
International Iberian Nanotechnology Labor…

34 PUBLICATIONS   **348** CITATIONS

SEE PROFILE

Wei-Guo Song
Chinese Academy of Sciences

110 PUBLICATIONS   **4,628** CITATIONS

SEE PROFILE

Programmed Fabrication of Metal Oxides Nanostructures Using Dual Templates to Spatially Disperse Metal Oxide Nanocrystals

Le-Sheng Zhang, Ling-Yan Jiang, Chao-Qiu Chen, Wei Li, Wei-Guo Song,* and Yu-Guo Guo*

Beijing National Laboratory for Molecular Sciences (*BNLMS*); *Institute of Chemistry, Chinese Academy of Sciences, Beijing, 100190, P. R. China*

Multiwalled carbon nanotubes (MWCNTs) and metal oxide composites, including MWCNTs@SnO_2, MWCNTs@ZrO_2, MWCNTs@Fe_2O_3, as well as corresponding metal oxides (MO) hollow structure consisted of SnO_2, ZrO_2, or CeO_2 metal oxide single crystals, respectively, are produced using porous carbonaceous coating and multiwalled carbon nanotube core as dual templates. The synthesis procedure involves programmed steps in which the templates are removed in a controlled sequence. The carbonaceous layer coated on MWCNTs provides porous surface for the adsorption of metal oxide precursors and a buffer zone to help the dispersion of metal oxide nanocrystals. The MWCNTs provide mechanical supports during the whole process before they are removed. MWCNTs@MO nanocomposite are obtained by the removal of the porous carbonaceous layer, and metal oxides hollow structure is produced after the removal of the MWCNTs. MWCNTs@SnO_2 nanocomposite shows excellent lithium storage property as anode material for lithium-ion batteries, and SnO_2 hollow structure shows high sensitivity and response rate as gas sensor material.

Introduction

Metal oxides have been very important materials in catalysis,[1,2] gas sensors,[3,4] and energy conversions.[5] It is desirable to produce metal oxide materials with large surface area and preferred morphologies that prompt mass transfer of the species. An excellent approach is to synthesize metal oxide nanocrystals and assemble them into certain uniform morphologies. However, because of the high surface energy of the nanocrystals, aggregation often occurs with them, resulting in irregular morphologies and limiting their applications. Three approaches were usually used to prevent the undesired aggregation of the nanocrystals. First is to fabricate metal oxide materials with pore structures in nanometer scale,[6,7] while preparing highly crystalline pore walls is still very difficult.[7] The second method is to assemble the nanoparticles into hierarchical structures with the help of surfactants.[8]

The third way is to disperse the metal oxides nanocrystals on a support with desired structures.[9]

When nanoparticles are dispersed on a supporting material, the support provides both surface for dispersion and mechanical support for the nanoparticles. In some applications such as lithium-ion batteries and gas sensors, the support also provides critical electron and ion diffusion courses.[10,11] Carbon nanotubes (CNTs) have been considered as an excellent choice as the support due to its structural, electronic, mechanical, and optical properties.[12] Several methods were developed to produce CNT supported composite materials. These methods are usually used for noble metal nanoparticles because mono dispersed noble metal nanoparticles can be generated under mild conditions in solution, and have strong interactions with functional groups on the CNT surface. However, it is difficult to produce dispersed metal oxides nanoparticles on CNTs. CNTs' surface is hydrophobic, in order to have strong bind between the metal oxide precursor and the CNT support (template), organic metal compounds and organic solvents are often used.[13-15]

*Corresponding author. E-mail: wsong@iccas.ac.cn (W.-G.S.); ygguo@iccas.ac.cn (Y.-G.G.).
(1) Cheng, F. Y.; Ma, H.; Li, Y. M.; Chen, J. *Inorg. Chem.* **2007**, *46*, 788.
(2) Liang, H. P.; Zhang, H. M.; Hu, J. S.; Guo, Y. G.; Wan, L. J.; Bai, C. L. *Angew. Chem., Int. Edit.* **2004**, *43*, 1540.
(3) Martinez, C. J.; Hockey, B.; Montgomery, C. B.; Semancik, S. *Langmuir* **2005**, *21*, 7937.
(4) Li, B. X.; Xie, Y.; Jing, M.; Rong, G. X.; Tang, Y. C.; Zhang, G. Z. *Langmuir* **2006**, *22*, 9380.
(5) Palomares, E.; Clifford, J. N.; Haque, S. A.; Lutz, T.; Durrant, J. R. *J. Am. Chem. Soc.* **2003**, *125*, 475.
(6) Yang, P. D.; Zhao, D. Y.; Margolese, D. I.; Chmelka, B. F.; Stucky, G. D. *Nature* **1998**, *396*, 152.
(7) Ba, J. H.; Polleux, J.; Antonietti, M.; Niederberger, M. *Adv. Mater.* **2005**, *17*, 2509.
(8) Yang, X. Y.; Li, Y.; Tendeloo, G. V.; Xiao, F. S.; Su, B. L. *Adv. Mater.* **2009**, *21*, 1368.

(9) Lou, X. W.; Archer, L. A.; Yang, Z. C. *Adv. Mater.* **2008**, *20*, 3971.
(10) Zhang, H. X.; Feng, C.; Zhai, Y. C.; Jiang, K. L.; Li, Q. Q.; Fan, S. S. *Adv. Mater.* **2009**, *21*, 2299.
(11) Lu, G. H.; Ocola, L. E.; Chen, J. H. *Adv. Mater.* **2009**, *21*, 2487.
(12) Georgakilas, V.; Gournis, D.; Tzitzios, V.; Pasquato, L.; Guldi, D. M.; Prato, M. *J. Mater. Chem.* **2007**, *17*, 2679.
(13) Yuan, R. S.; Fu, X. Z.; Wang, X. C.; Liu, P.; Wu, L.; Xu, Y. M.; Wang, X. X.; Wang, Z. Y. *Chem. Mater.* **2006**, *18*, 4700.
(14) Ogihara, H.; Sadakane, M.; Nodasaka, Y.; Ueda, W. *Chem. Mater.* **2006**, *18*, 4981.
(15) Zhang, D. S.; Fu, H. X.; Shi, L. Y.; Fang, J. H.; Li, Q. *J. Solid State Chem.* **2007**, *180*, 654.

Article

Chem. Mater., Vol. 22, No. 2, 2010 415

For supported metal oxide materials, if the loading is high enough so that the metal oxide nanoparticles forms mulitlayers on the support, then hollow structures can be formed when the support is removed. Hollow structured metal oxide materials may be very useful in applications where the volume of the materials changes significantly, for example, during the lithium ion uptake and release cycle.[16,17] Many methods had been developed to fabricate metal oxide hollow structures, including polyol-mediated method,[18] oxidation-coordination-assisted dissolution method,[19] hydrothermal method,[20] and sacrificial templating method.[13−15,21−30] Among these methods, template route using hard (solid) templates is perhaps the most effective method.[9] Hard template method for hollow materials is essentially a two step method. The first step is to load the desired particles on the support (template), and then in the second step, the support (template) is removed. In recent years, several supporting templates, such as carbonaceous sphere,[31] hydrogels,[21] carbon nanofiber,[13,14,24−26] carbon nanotubes (CNTs)[15,27−29] as sacrificial supporting templates were used to produce hollow tubes with fixed internal diameter and variable wall thickness. Carbonaceous spheres and fibers are porous and hydrophilic, so that the inorganic metal oxide precursor solution can readily mix with the template.[17,24,32] Metal oxide hollow structures are generated when the templates are removed by combustion. However, it is very difficult to control the sizes of the materials.[31,32] In addition, the hollow structure often collapses during the removal of the templates.

To overcome these problems, we developed a dual templates route to fabricate a series of metal oxides on MWCNTs composite materials (MWCNTs@MO) and metal oxide hollow structure, including SnO_2, ZrO_2, Fe_2O_3, and CeO_2, using carbonaceous carbon layer and MWCNTs core as dual templates. With dual templates

Scheme 1. Schematic Illustration of the Programmed Fabrication Process of Metal Oxide Hollow Structure Using Carbonaceous Layer Coated MWCNTs Dual Templates
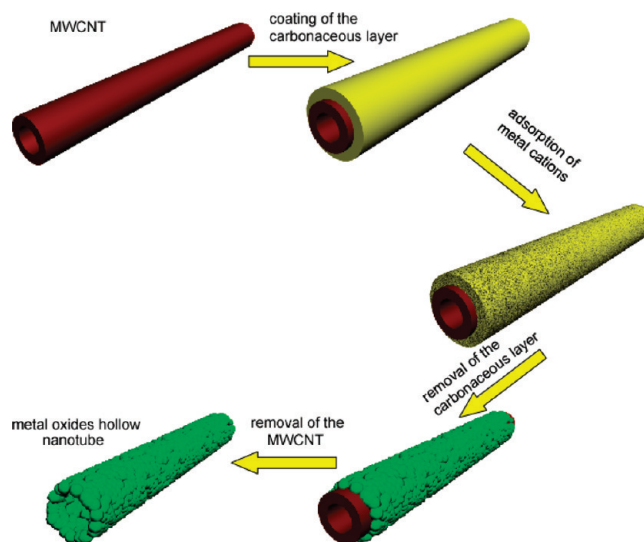
we are able to spatially and chronically separate the whole process into programmed steps. The overall synthesis procedure employed for the preparation of MWCNTs@MO composites and metal oxide hollow structure was illustrated in Scheme 1. During the hydrothermal treatment, the carbonaceous layer was coated on the carbon nanotube to form dual templates. Then, metal cations permeate into the carbonaceous layer to load the metal oxide precursors into the coating layer. By calcinating the sample at a relatively low temperature (280 or 400 °C) in air, the metal salts were converted into metal oxides. Along this metal oxide forming process, the carbonaceous layer was removed; while MWCNTs, which can sustain mild heating, remain intact, thus MWCNTs@MO composites were obtained. When the calcinations temperature was elevated to 550 °C, MWCNTs were combusted, leaving metal oxide nanocrystals stacking with each other to form metal oxide hollow structure.

This approach is reproducible and applies to several metal oxides, resulting in several MWCNTs@MO and metal oxides hollow structure, which show excellent properties in sensor and lithium ion battery applications.

Experimental Section

Materials. Multiwalled carbon nanotubes (MWCNTs) was purchased from Shenzhen Nanotech Port Co. Ltd. and was pretreated in 6 M nitric acid for 12 h. All other reagents were purchased from Beijing Chemical Reagent Corporation, China, and used as received.

Preparation of Dual Templates. In a typical procedure, glucose (1.5 g) was dissolved in an aqueous solution of 10 mL deionized water and 5 mL ethanol. Thirty mg of MWCNT was then ultrasonically dispersed in the solution, forming dark but homogeneous suspension. The mixture was then sealed in a 40 mL autoclave with a Teflon linear and was heated to 190 °C for 6 h, resulting in a dark purple mixture, which were collected by centrifugation, and washed with four cycles of washing with

(16) Zhang, W. M.; Hu, J. S.; Guo, Y. G.; Zheng, S. F.; Zhong, L. S.; Song, W. G.; Wan, L. *J. Adv. Mater.* **2008**, *20*, 1160.
(17) Demir-Cakan, R.; Hu, Y. S.; Antonietti, M.; Maier, J.; Titirici, M. M. *Chem. Mater.* **2008**, *20*, 1227.
(18) Wang, Y. L.; Jiang, X. C.; Xia, Y. N. *J. Am. Chem. Soc.* **2003**, *125*, 16176.
(19) Zhou, K. B.; Yang, Z. Q.; Yang, S. *Chem. Mater.* **2007**, *19*, 1215.
(20) Han, W. Q.; Wu, L. J.; Zhu, Y. M. *J. Am. Chem. Soc.* **2005**, *127*, 12814.
(21) Gundiah, G.; Mukhopadhyay, S.; Tumkurkar, U. G.; Govindaraj, A.; Maitra, U.; Rao, C. N. R. *J. Mater. Chem.* **2003**, *13*, 2118.
(22) Dickey, M. D.; Weiss, E. A.; Smythe, E. J.; Chiechi, R. C.; Capasso, F.; Whitesides, G. M. *ACS Nano* **2008**, *2*, 800.
(23) Chen, J.; Xu, L. N.; Li, W. Y.; Gou, X. L. *Adv. Mater.* **2005**, *17*, 582.
(24) Qian, H. S.; Yu, S. H.; Ren, L.; Yang, Y. P.; Zhang, W. *Nanotechnology* **2006**, *17*, 5995.
(25) Qian, H. S.; Yu, S. H.; Luo, L. B.; Gong, J. Y.; Fei, L. F.; Liu, X. M. *Chem. Mater.* **2006**, *18*, 2102.
(26) Huang, J.; Matsunaga, N.; Shimanoe, K.; Yamazoe, N.; Kunitake, T. *Chem. Mater.* **2005**, *17*, 3513.
(27) Satishkumar, B. C.; Govindaraj, A.; Nath, M.; Rao, C. N. R. *J. Mater. Chem.* **2000**, *10*, 2115.
(28) Rao, C. N. R.; Satishkumar, B. C.; Govindaraj, A. *Chem. Commun.* **1997**, 1581.
(29) Ajayan, P. M.; Stephan, O.; Redlich, P.; Colliex, C. *Nature* **1995**, *375*, 564.
(30) Ma, Z.; Liu, Q.; Cui, Z. M.; Bian, S. W.; Song, W. G. *J. Phys. Chem. C* **2008**, *112*, 8875.
(31) Sun, X. M.; Liu, J. F.; Li, Y. D. *Chem.−Eur. J.* **2006**, *12*, 2039.
(32) Titirici, M. M.; Antonietti, M.; Thomas, A. *Chem. Mater.* **2006**, *18*, 3808.

water or ethanol. Finally the samples were dried at 80 °C overnight.

Synthesis of MWCNTs@MO Composites and Metal Oxide Nanostructure. Typically, the desired metal salt ($SnCl_4$, Fe-$(NO_3)_3$, $Ce(NO_3)$, etc.) was dissolved in 20 mL ethanol (forming 0.2 M solution). In the case of $ZrO(NO_3)_2$, which has low solubility in ethanol, a mixture solution of 15 mL of ethanol and 5 mL of deionized water was used.

Oven-dried dual template (60 mg) was then dispersed in the above-mentioned metal salt solutions under ultrasonication. The ultrasonication continued for 30 min to ensure saturation of the metal salt solution into the carbonaceous coating layer. The black-brown sample was recovered from the solution, washed and then dried at 80 °C for 12 h. MWCNTs@MO composites were produced by calcinating the sample at 280 or 400 °C for 4 h. Corresponding metal oxide hollow structure was obtained after calcination of the MWCNTs@MO composites at 550 °C for 6 h.

Characterization of the Samples. The microscopic features of the samples were characterized by scanning electron microscopy (SEM, JEOL-6701F) equipped with an energy-dispersive X-ray analyzer, transmission electron microscopy (TEM, JEOL JEM-1011), and high-resolution TEM (HRTEM, JEOL JEM-2010). X-ray powder diffraction (XRD) patterns were collected on a Rigaku D/max-2500 diffractometer with Cu KR radiation (λ = 0.1542 nm) at 40 kV and 100 mA. The TGA measurement was carried out in air at a heating rate of 2 °C min^{-1} using a Perkin-Elmer Diamond TG/DTA Instruments. The weight content of the SnO_2 in the composites was obtained from the inductively coupled plasma emission spectrometer (ICP-AES, Shimadzu) analysis. The SnO_2 on the composite was dissolved by a mixed acid solution (HCl/HNO_3 = 3:1) and the quality of Sn^{4+} in the solution were then analyzed by elemental analysis using ICP-AES instrument.

Electrochemical experiments were carried out in Swagelok-type cells. The working electrode was fabricated by casting a slurry composed of 80 wt % active material (MWCNTs@SnO_2, commercial SnO_2), 10 wt % poly(vinylidene fluoride) (PVDF), and 10 wt % carbon black onto a copper foil (99.6%, Good-fellow). The electrolyte consisted of a solution of 1 M $LiPF_6$ in ethylene carbonate (EC)/dimethyl carbonate (DMC)/diethyl carbonate (DEC) (1:1:1, in wt %) obtained from Novolyte Technologies (Suzhou) Co., Ltd. Lithium foil was used as the counter electrode. A glass fiber (GF/D) from Whatman was used as a separator. All the cells were assembled in an argon-filled glovebox and were tested on an Arbin BT2000 system at a rate of C/10 in the voltage range of 0.02−3.0 V (vs Li$^+$/Li).

The gas-sensitivity measurements were carried out in a homemade sensor testing system, and the sensor film were constructed by depositing a drop of as-prepared ethanol suspension of tin oxide on a commercial sensor electrode (UST, Germany). Hydrogen was used as the testing gas and was introduced into the testing chamber by mass flow controller. Measurements were carried out at 250 °C, 320 °C, 380 °C, respectively.

Results and Discussion

Preparation of MWCNTs@SnO_2 Nanocomposite and SnO_2 Hollow Structure. TEM image of the dual template (Figure 1a) reveals the presence of a layer of carbonaceous coating and the MWCNT core. The carbonaceous coating region is greyer than the MWCNTs part, indicating that the coating section is quite loose and with about 80 nm in thickness. Since the carbonaceous layer is
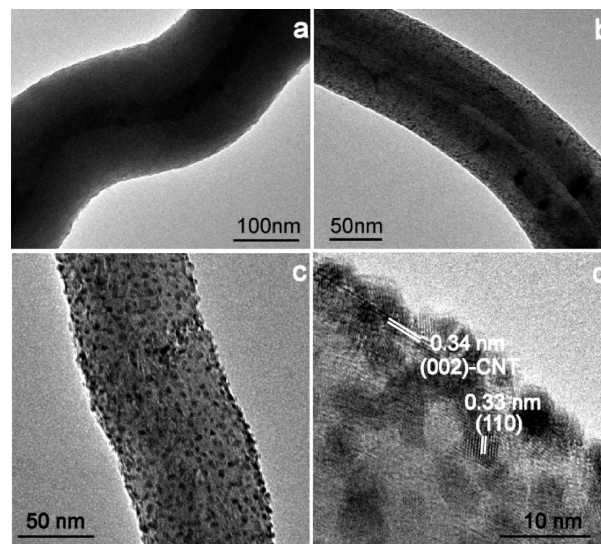

Figure 1. (a) TEM image of the carbonaceous layer coated MWCNT. (b) TEM image of carbonaceous layer coated MWCNT dual template after mixing with $SnCl_4$ solution and heated in air at 400 °C for 1 h. (c) TEM image of MWCNTs@SnO_2 nanocomposites after 4 h heating in air. (d) HRTEM image of part of MWCNTs@SnO_2 nanocomposites after 4 h heating in air.

produced in liquid, it is hard for glucose solution to enter the inner space of the CNTs. We believe that carbonaceous layer is coated only on the outer surface of the CNTs. The carbonaceous layer, formed by the carbonization of glucose under hydrothermal condition, is hydrophilic because of the abundant surface functional groups such as —OH and C=O groups, which can attract the metal ions.[33] When the coat layer is mixed with metal salt solutions, the solution immediately permeates into the pores of the loose carbonaceous layer. As the functional groups and the pores are evenly distributed throughout the coating, metal ions are thus spatially dispersed within the coating layer. This is crucial in obtaining highly dispersed metal oxide nanoparticles.

Figure 1b and c shows MWCNTs@SnO_2 composite treated in muffle furnace at 400 °C for 1 and 4 h, respectively. After 1 h of calcination, the carbonaceous layer is partially removed and a much thinner coating layer (20 nm) remains. SnO_2 nanocrystals (Figure 1b) trapped in the carbonaceous layer can be seen. After 4 h, the carbonaceous layer is completely removed. SnO_2 nanocrystals with the size of about 4 nm were formed and uniformly loaded on the MWCNT as shown in Figure 1c. No aggregation of SnO_2 nanocrystals is observed. High resolution TEM images shown in Figure 1d indicates that the SnO_2 nanocrystals exhibit (110) face of the rutile phase with a lattice space of 0.33 nm. The lattice fringe of 0.34 nm from the 002 face of the MWCNTs can also be seen (JCPDS 75−1621), proofing that the carbonaceous layer is completely removed. During the process in Figure 1a−c, porous carbonaceous carbon layer provides spaces for the metal oxide nanoparticles to form without aggregation. During the removal of the carbonaceous layer, the metal oxide nanoparticles gradually

(33) Sun, X. M.; Li, Y. D. *Angew. Chem., Int. Ed.* **2004**, *43*, 597.
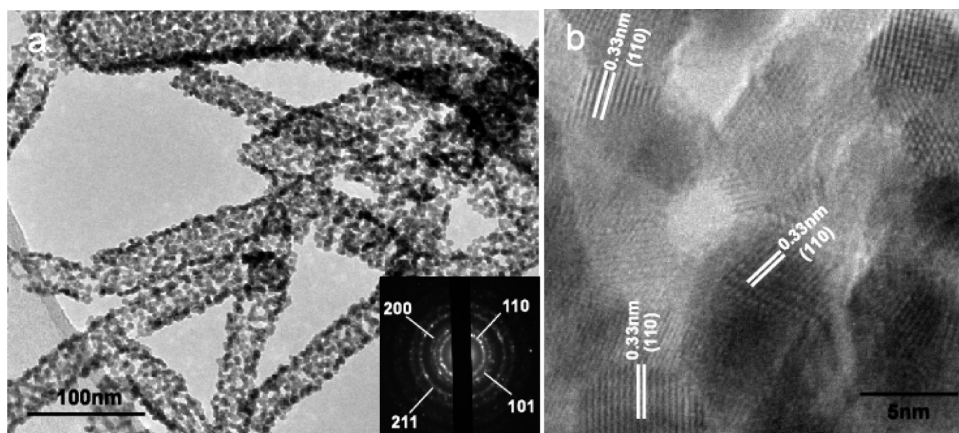
Figure 2. (a) TEM image of SnO$_2$ hollow structure obtained after removal of carbon coated MWCNT template. The inset shows a typical SAED pattern, which could be indexed to SnO$_2$. (b) High resolution TEM image of part of (a).

reach the surface of the MWCNT core and stay there to form MWCNTs@MO composite. Since the metal oxide nanoparticles are well dispersed spatially in the carbonaceous layer, they are also well dispersed on the MWCNT surface (Figure 1c).

When the MWCNT template is removed at 550 °C, hollow structure consisting of SnO$_2$ nanoparticles are formed with diameters of about 40 nm (Figure 2a). The SnO$_2$ nanoparticles' grain size was between 5 and 7 nm. The diameter of the resulting SnO$_2$ nanotubular structure is smaller than the MWCNTs template, which has a diameter of about 60 nm. The SAED pattern (inset Figure 2a) and the XRD pattern (Supporting Information (SI) Figure S1 and JCPDS 41-1445) confirm that the obtained SnO$_2$ hollow structure is rutile phase. HRTEM image (Figure 2b) shows that the tube wall is composed of SnO$_2$ nanocrystals with well-defined lattices with a spacing of 0.33 nm from the (110) face of the rutile phase. The wall is loose, as shown in Figure 2a and b, suggesting that most SnO$_2$ nanocrystals can be accessed.

The TG-DTA curves of the Sn^{4+} loaded dual template (carbonaceous carbon coated MWCNT) shows a three step mass loss process (see SI Figure S2). The first weight loss occurred at around 100 °C and is due to the loss of adsorbed water. A broad peak from 200 to 400 °C is caused by the combustion of amorphous carbonaceous layer. Finally, the removal of MWCNTs occurred from about 450 to 650 °C. As indicated in the TG analysis, carbon residues may still exist in the sample even after 700 °C calcination in air. However, the amount of the weight loss after 550 °C is lower than 10%, thus we believe the amount of the carbon residues after calcination at 550 °C for 6 h would be very small.

To highlight the role of the coated carbonaceous layer, a controlled experiment was carried out using uncoated MWCNT as single template to produce SnO$_2$ hollow structure. Only few SnO$_2$ bulk crystals were found (see SI, Figure S3). Uncoated MWCNTs surface is hydrophobic, thus aqueous solution of SnCl$_4$ can not stay on it. The carbonaceous coating provides a hydrophilic space for aqueous solution to be evenly loaded around the MWCNT core.

Preparation of MWCNTs@ZrO$_2$, MWCNTs@Fe$_2$O$_3$ Nanocomposites and ZrO$_2$, CeO$_2$ Hollow Structure. This approach was extended to fabricate other MWCNTs@MO nanocomposites and metal oxide hollow structure.[34-37] We found out that the chemical nature of the metal oxide determines the outcome of this method. In case of ZrO$_2$, TEM images (SI Figure S4) shows that MWCNTs@ZrO$_2$ composite as well as ZrO$_2$ nanotubular structures is formed with similar morphology to SnO$_2$ product. After the heat treatment step to remove the carbonaceous layer, ZrO$_2$ nanocrystal with the size of about 3−5 nm were uniformly dispersed on the surface of MWCNTs@ZrO$_2$ composite. ZrO$_2$ hollow structure is consisted of ZrO$_2$ nanoparticles of both monoclinic and cubic phases (SI Figure S5 and JCPDS 37-1484, 49-1642). The HRTEM image (SI Figure S4d) shows two different lattice space, 0.284 and 0.296 nm, corresponding to the (111) face of the monoclinic phase and cubic phase, respectively.

For Fe$_2$O$_3$, a relative lower temperature (280 °C) was used to fabricate the MWCNTs@Fe$_2$O$_3$ composite. Figure 3a shows that the Fe$_2$O$_3$ nanoparticles were evenly loaded on the MWCNT after the selective removal of the carbonaceous template. However, no Fe$_2$O$_3$ hollow structure was obtained. Instead, Fe$_2$O$_3$ nanorods with hematite phase (JCPDS 87-1164) were produced after the high temperature removal of MWCNT template, as shown in Figure 3b. Inset Figure b1 and b2 further confirms the single crystals structure of the iron oxide nanorods with lattice space of 0.269 nm from (104) face, and discrete dots in SAED from (104) and (021) face diffraction. During the removal of MWCNTs template, it is likely iron oxide nanocrystals are reduced to iron nanodroplets, which readily merged to form rod like structures along the MWCNT axis. The iron nanorods

(34) Wang, D. H.; Ma, Z.; Dai, S.; Liu, J.; Nie, Z. M.; Engelhard, M. H.; Huo, Q. S.; Wang, C. M.; Kou, R. *J. Phys. Chem. C* **2008**, *112*, 13499.
(35) Mayernick, A. D.; Janik, M. J. *J. Phys. Chem. C* **2008**, *112*, 14955.
(36) Bronkema, J. L.; Bell, A. T. *J. Phys. Chem. C* **2008**, *112*, 6404.
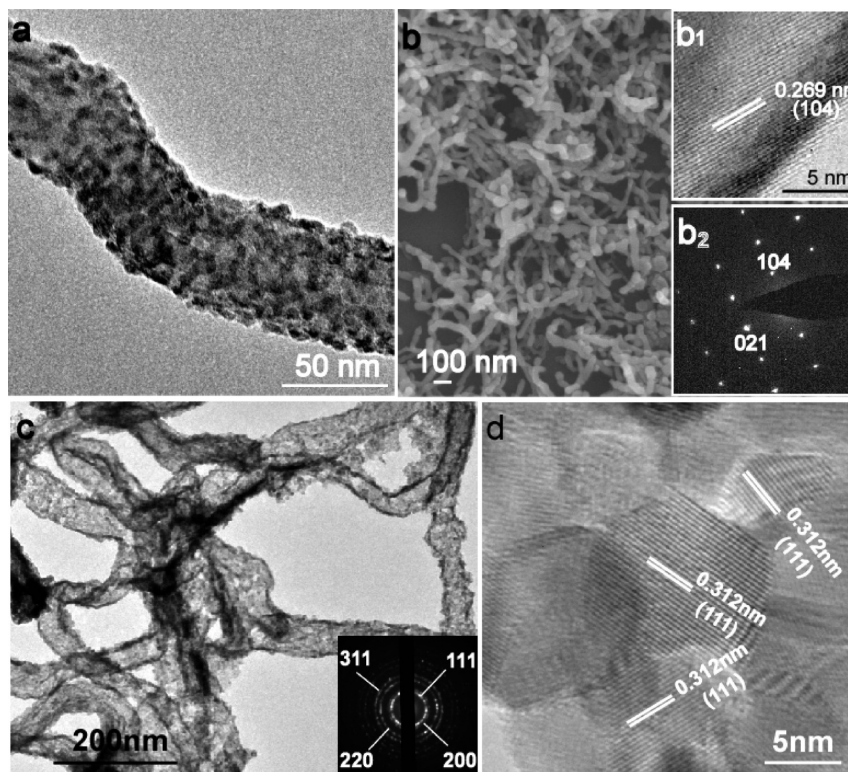(37) Zhong, D. K.; Sun, J.; Inumaru, H.; Gamelin, D. R. *J. Am. Chem. Soc.* **2009**, *131*, 6086.

Figure 3. (a) TEM image of MWCNTs@Fe$_2$O$_3$ nanocomposites. (b) SEM image of Fe$_2$O$_3$ nanorod, inset b$_1$ and b$_2$ shows the HRTEM and the SAED pattern of part of the nanorod, respectively. (c) and (d) TEM image of CeO$_2$ hollow structure and HRTEM of part of (c).

are oxidized again to Fe$_2$O$_3$ when MWCNTs are completely removed.

Things become interesting for CeO$_2$; as only CeO$_2$ hollow structure can be produced. We could not selectively remove carbonaceous layer by heating at any temperature. The dual templates are either combusted together at relatively high temperatures or intact at lower temperatures. CeO$_2$ is an excellent combustion catalyst,[38] thus MWCNTs and carbonaceous coating are combusted simultaneously. The obtained CeO$_2$ hollow structure is consisted of nanoparticles with face-centered cubic structure (Figure 3c). The lattice space of 0.312 nm is observed in HRTEM images for CeO$_2$ nanocrystals (Figure 3d), corresponding to the (111) face of the face-centered cubic structure (JCPDS 34-0394).

Electrochemical Application. We conducted a preliminary investigation using MWCNTs@SnO$_2$ as the anode material of lithium-ion batteries. Its performance was compared with that of commercial bare SnO$_2$ powder. The nanotubular structure SnO$_2$ was not tested since the grinding process during the preparation of anode material may destroy the hollow structure. The results were illustrated in Figure 4. The commercial SnO$_2$ powder shows a specific charge capacity of 838.4 mA h g^{-1} in the first cycle. After 45 cycles, however, its capacity decreased dramatically and reached 148 mA h g^{-1}, which was only 17.7% of its initial capacity. On the contrary, the MWCNTs@SnO$_2$ composite electrode consisting of 25%
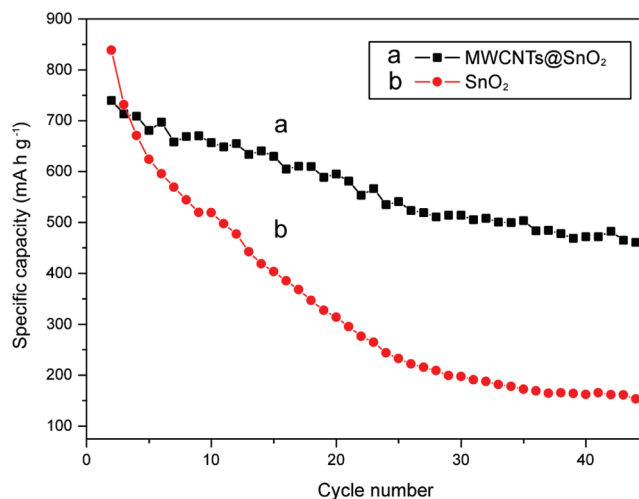

Figure 4. Cycle performance of (a) MWCNTs@SnO$_2$, and (b) commercial SnO$_2$ at a rate of C/10.

SnO$_2$ shows a much improved cycling performance. The specific charge capacity of the MWCNTs@SnO$_2$ composite was 739.5 mA h g^{-1} in the first cycle and still as high as 464 mA h g^{-1} after 45 cycles.

The poor cycling performance of bare SnO$_2$ is attributed to the huge volume variation during Li uptake/ release cycles, which causes structural damage of the SnO$_2$ particles.[39,40] For pure nanosized SnO$_2$ particles, the problem may be released at the expense of successive

(38) Gonzalez-Rovira., L.; Sanchez-Amaya, J. M.; Lopez-Haro, M.; del Rio, E.; Hungria, A. B.; Midgley, P.; Calvino, J. J.; Bernal, S.; Botana, F. J. *Nano Lett.* **2009**, *9*, 1395.

(39) Wen, Z. H.; Wang, Q.; Zhang, Q.; Li, J. H. *Adv. Funct. Mater.* **2007**, *17*, 2772.

(40) Derrien, G.; Hassoun, J.; Panero, S.; Scrosati, B. *Adv. Mater.* **2007**, *19*, 2336.

agglomeration of the particles, which also leads to capacity fading. It has been reported that pinning nanosized alloy particles on carbon sphere surface tightly is an effective way to enhance the dimensional stability of nanoalloy particles during cycling.[41] In the case of MWCNTs@SnO_2 composite, the much enhanced cycling performance can be attributed to the highly dispersed SnO_2 nanoparticles as well as the supporting material of MWCNTs. While the former could more easily accommodate the volume changes and prevents the pulverization of SnO_2, the latter provide a similar pining effect as those carbon spheres, which can effectively prevents the electrochemical aggregation of SnO_2 nanoparticles during electrochemical cycles. In addition, the MWCNTs in the composite enhance the electron conductivity of the whole electrode and reduce the ohmic loss among active particles.

Sensor Application. The unique hollow structure morphology of the SnO_2 is desirable in surface-related applications, such as gas sensor.[42,43] The small grain size (5−7 nm) and tubular structure would allow full contact between SnO_2 surface and gas molecules, and fast diffusion of target gas on the sensing materials. The sensitivity of the obtained SnO_2 hollow structure against hydrogen was investigated and shown in Figure 5(a). The gas sensitivity, S_g is calculated from R_0/R, where R_0 and R are the electrical resistances for the sensor in air and in sensing gas.[23] The sensitivity increases from 1.82 to 3.34 when the hydrogen gas concentration is increased from 10 to 50 ppm at 380 °C. Comparison between SnO_2 hollow structures and commercial SnO_2 are provided in Figure 5a, which shows that the response from hollow structures is larger. More importantly, the signal drifting is much smaller from hollow structure than from commercial SnO_2. Signal drifting is one of the issues for gas sensor. Better performance from hollow structure is likely due to fast and full recovery of the sensing material when hydrogen flow is cut off. The response time and recovery time of the sensing material is an important feature.[44] The results reveled in Figure 5(b) indicates that the response time and recovery time is as short as 24 s (T_1) and 27 s (T_2), respectively, implying that SnO_2 hollow structure was a promising nanomaterial in fabricating quick response and recovery gas sensor.

Conclusion

In conclusion, we developed a programmed dual template method to fabricate a series of MWCNTs@MO nanocomposites, including MWCNTs@SnO_2, MWCNTs@ZrO_2, MWCNTs@Fe_2O_3, and metal oxide hollow structure including SnO_2, CeO_2. The metal oxide nanocrystals are highly dispersed and stable on the MWCNTs
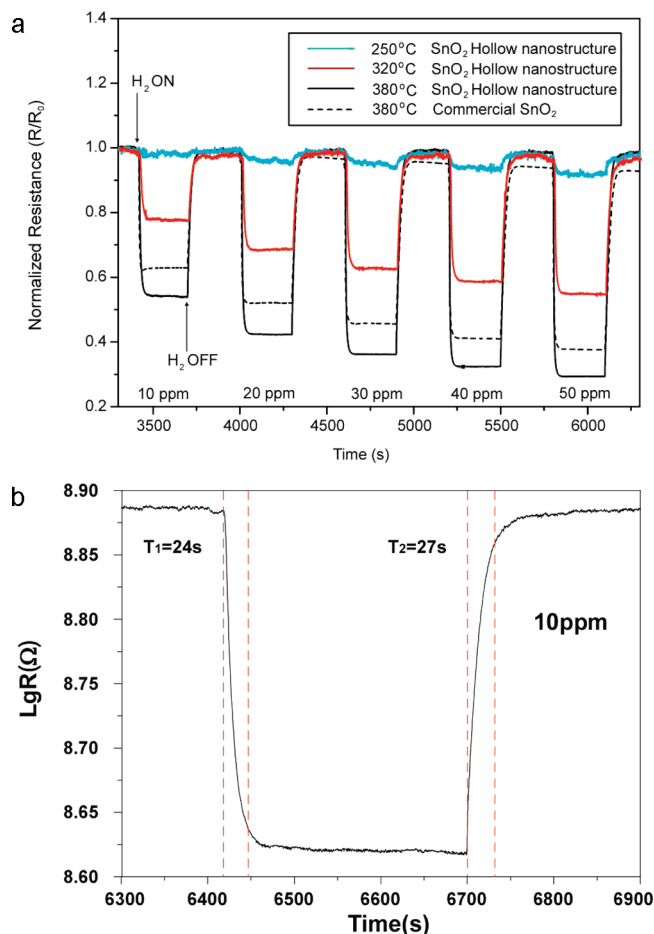

Figure 5. (a) Typical response curves of hydrogen with increasing concentrations (10−50 ppm) at different working temperature. R_0 and R represent the electrical resistances for the sensor in air and in sensing gas. (b) Partly magnified response curves of SnO_2 hollow nanostructure operated at 380 °C in a concentration of 10 ppm.

surface. The dual template is consisted of a MWCNTs core and a carbonaceous coating layer. The outside carbonaceous layer provides hydrophilic space and affinity for inorganic metal oxide precursors. The MWCNTs provides the structural supports during the whole procedure before they were removed. MWCNTs@SnO_2 and SnO_2 hollow structure were tested. MWCNTs@SnO_2 shows excellent cycling performance in lithium ion battery and SnO_2 hollow structure has high sensitivity, fast response and recovery rate in hydrogen sensing.

Supporting Information Available: XRD patterns of SnO_2, ZrO_2, Fe_2O_3, and CeO_2 hollow structure. TG-DTA curves of the Sn^{4+} loaded dual template and TEM image of SnO_2 nanoparticles loaded on pristine MWCNTs. TEM images of the process of the formation of Fe_2O_3 nanorods and TEM image of ZrO_2 hollow structure. This material is available free of charge via the Internet at http://pubs.acs.org.

(41) Li, H.; Shi, L.; Wang, Q.; Chen, L.; Huang, X. *Solid State Ionics* **2002**, *148*, 247.
(42) Yu, C.; Hao, Q.; Saha, S.; Shi, L.; Kong, X. Y.; Wang, Z. L. *Appl. Phys. Lett.* **2005**, *86*, 3.
(43) Comini, E.; Faglia, G.; Sberveglieri, G.; Pan, Z. W.; Wang, Z. L. *Appl. Phys. Lett.* **2002**, *81*, 1869.
(44) Liu, J. F.; Wang, X.; Peng, Q.; Li, Y. D. *Adv. Mater.* **2005**, *17*, 764.